Rheol Acta (2011) 50:403–422
DOI 10.1007/s00397-011-0544-3

ORIGINAL CONTRIBUTION

Immiscible Newtonian displacement by a viscoplastic material in a capillary plane channel

Jackson F. Freitas · Edson J. Soares · Roney Leon Thompson

Received: 14 May 2010 / Revised: 1 March 2011 / Accepted: 12 March 2011 / Published online: 28 April 2011

Abstract The immiscible displacement in a capillary plane channel of a Newtonian liquid by a viscoplastic one that obeys a Papanastasiou's constitutive equation is numerically analyzed. An elliptic mesh generation technique, coupled with the Galerkin finite element method is used to determine the velocity field and the configuration of the interface between the two materials. We investigate the displacement efficiency and the flow patterns of the problem as functions of the dimensionless parameters that govern the problem: the capillary number (Ca), the viscosity ratio of the two fluids (N_η) and the yield number, (τ_0'). The numerical results showed that for a fixed viscosity ratio, the fraction of mass attached to the wall is a decreasing function of τ_0'. We constructed maps of streamlines in the Cartesian space defined by τ_0' and Ca for fixed viscosity ratios in order to capture the rough location of bypass and recirculating flow regimes. Higher yield number values induce bypass flow regimes, especially for high Ca. The dimensionless forms of the momentum conservation equation and the force balance at the interface were essential for the understanding of the role played by the dimensionless numbers that govern the problem.

Keywords Interface tension · Finite element analysis · Viscoplastic material · Displacement efficiency · Unyielded zones

This paper was presented at Viscoplastic Fluids: From Theory to Application, 1–5 November 2009, Limassol, Cyprus.

J. F. Freitas · E. J. Soares
LFTC, Department of Mechanical Engineering, Universidade Federal do Espirito Santo, Avenida Fernando Ferrari, 514, Goiabeiras, Victoria, 29075-910, Espírito Santo, Brazil

R. L. Thompson (✉)
LFTC-LMTA, Department of Mechanical Engineering (PGMEC), Universidade Federal Fluminense, Rua Passo da Patria 156, 24210-240, Niteroi, Rio de Janeiro, Brazil
e-mail: rthompson@mec.uff.br

Introduction

The displacement of a fluid by another is an important problem in fluid mechanics that has received significant attention from the literature. Among the numerous industrial applications, we focus our attention on the oil recovery in porous media. This process is sketched in Fig. 1. In this case, the mechanical properties of the oil that fills the rocks of the reservoir are fixed. On the other hand, one can test different injected materials so as to take advantage of the rheological character of the displacing fluid to optimize this process.

The idealized problem conceived to model the industrial process described can be simplified into a 2-D approach in two manners: the fluid–fluid displacement in a capillary tube or in a capillary plane channel, often called Hele-Shaw cell. The former represents a useful simplification for the case where the cross area of the porous passage has an aspect ratio around the unity while the latter is more adequate to mimic the case of high values of aspect ratio. A comparison between the axisymmetric and Cartesian approaches for the case of Newtonian–Newtonian displacement can be found in Freitas et al. (2011).

The gas–liquid (Newtonian) displacement has received considerable attention in the literature and was

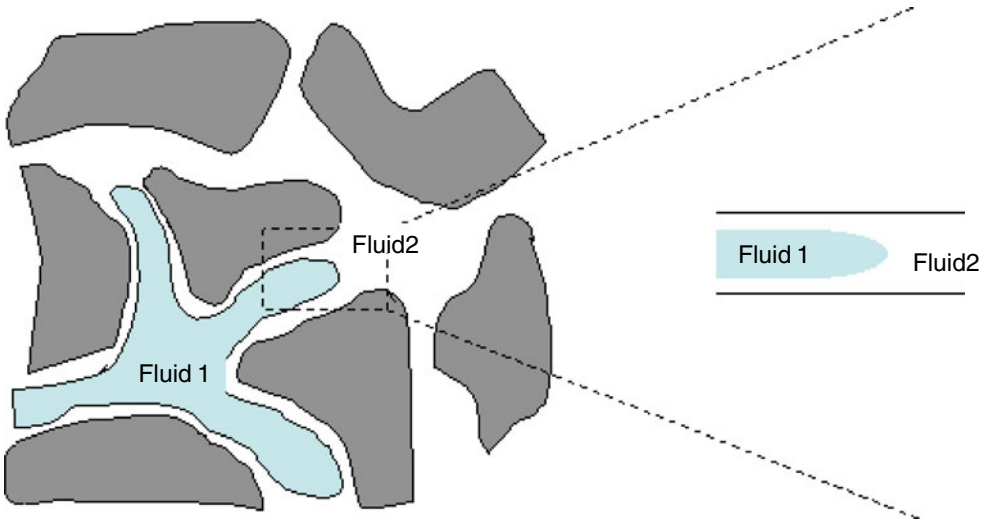

Fig. 1 On the *left*: injection of phase 1 into a porous media filled with phase 2. On the *right*: simplified 2-D problem

investigated by several authors such as Fairbrother and Stubbs (1935) (experimentally), Bretherton (1961) (theoretically), Taylor (1961) (experimentally), Cox (1962) (experimentally), Park and Homsky (1984) (theoretically), Chen (1986) (experimentally), Martinez and Udell (1989) (numerically), and Giavedoni and Saita (1997) (numerically).

The gas displacement of the non-Newtonian fluids has also received some attention. Hassager and Lauridsen (1998), Sousa et al. (2007) and Thompson et al. (2010) investigated the gas displacement of power-law fluids. Poslinski et al. (1995), Alexandrou and Entov (1997), Dimakopoulos and Tsamopoulos (2003), de Souza Mendes et al. (2007), Sousa et al. (2007), and Thompson et al. (2010) studied the problem of gas displacing viscoplastic materials. The gas displacement of viscoelastic materials was studied by Huzyak and Koelling (1997), Lee et al. (2002), Dimakopoulos and Tsamopoulos (2004), among others.

The liquid–liquid displacement of two immiscible Newtonian fluids has been investigated since the pioneering work of Goldsmith and Mason (1963). Since than, important contributions were made by Westborg and Hassager (1989), Martinez and Udell (1990), Hodges et al. (2004), Soares et al. (2005), Soares and Thompson (2009), and Freitas et al. (2011), among others. In the liquid–liquid displacement problem, the conservation equations are solved in the displacing fluid domain also and the force balance at the interface needs an additional term that takes into account the extra normal stress at the displacing fluid side, besides the pressure.

Papaioannou et al. (2009) investigated the conditions of wall detachment when the injected material is a viscoplastic Papanastasiou's material while the displaced fluid is a gas.

Allouche et al. (2000), Taghavi et al. (2009) and Malekmohammadi et al. (2010) investigated the liquid–liquid displacement when the two fluids are non-Newtonian. They recovered the immiscible problem as an approximation of the miscible one for the limit of high values of the Peclet number and, therefore, capillary effects were not analyzed.

A recent study of the Newtonian displacement by a non-Newtonian liquid when capillary stresses are important was conducted by Thompson and Soares (2010) for the case of power-law displacing fluid.

Viscoplastic materials are widely used in industrial processes. It is not an easy task to implement a numerical scheme to solve complex flows of yield stress materials in the sense originally conceived by Bingham (1916), i.e., with a vanishing rate of deformation when the applied stress is below the material yield stress. The options to implement an approximation of this kind of behavior are: (a) a bi-viscosity model, (b) a viscoplastic model with a regularization parameter, and (c) a viscoplastic physically regularized model.

Bi-viscosity models are characterized by a two-rule expression for the viscosity function: a very high value when the stress is below the yield stress and the classic expression proposed by Bingham (1916): $\eta = \mu_P + \frac{\tau_0}{\dot{\gamma}}$.

The models with a regularization parameter are inspired by the original work developed by Papanastasiou (1987). In this case, an ad hoc (regularization) parameter is introduced and the proposed model has a smooth transition between the region where the stress is below the material yield stress to the region where the stress is above the material yield stress. The choice of the regularization parameter is a matter of discussion in the literature. Important analyses on the subject are made by Frigaard and Nouar (2005) and Putz et al. (2009). Ideally the problem should be independent of the cho-

sen value. It is worth noticing that Zou et al. (2008) recommend a dimensionless regularization parameter of a thousand.

A first viscoplastic physically regularized model was presented by de Souza Mendes and Dutra (2004). In this case, the model is conceptually more aligned to the idea, discussed by Barnes (1999), that the yield stress does not bound a region where there is no deformation rate but is simply a level of stress below which the fluid has a very high level of viscosity. When the stress achieves the material yield stress, the microstructure starts to be destroyed and there is a dramatic viscosity decrease.

In the present work, we analyze the displacement of a Newtonian fluid by a Papanastasiou material in a plane channel. We focus our investigation on the influence of the yield number on the displacement efficiency and on the flow regimes that the solution presents.

Problem formulation

The scheme of the problem analyzed is depicted in Fig. 2. The reference frame is attached to the tip of the drop and, therefore, the wall moves with its velocity, U. The channel has a $2H_0$ gap. We assume that there is a part of the domain, region IV, where the flow is fully developed with a fixed distance from the centerline till the interface, H_b. With this assumption, the problem in this reference frame is steady. The flow is assumed to be isothermal, inertialess, and incompressible.

Governing equations

The governing equations are presented here in a dimensionless form using appropriate characteristic velocity and length scales, the wall velocity U and the half distance of the capillary gap, H_0, respectively, together with a characteristic stress, $\mu_2 U/H_0$, where μ_2 is the viscosity of the displaced Newtonian fluid. The conservation of mass equation is given by

$$\nabla^* \cdot \mathbf{u}_k^* = 0. \tag{1}$$

while the equation for conservation of momentum is given by

$$\nabla^* \cdot \mathbf{T}_k^* = -\nabla^* p_k^* + \nabla^* \cdot \mathbf{T}_\mathbf{k}^{\mathbf{E}*} = 0, \tag{2}$$

where the subscript $k = 1, 2$ labels the two materials considered. In Eq. 1, $\mathbf{u}_k^*$ is the dimensionless velocity vector, $\mathbf{u}_k = U\mathbf{u}_k^*$, and in Eq. 2, $\mathbf{T}_k^* = -p_k^*\mathbf{1} + \mathbf{T}_\mathbf{k}^{\mathbf{E}*}$ is the total dimensionless stress tensor, where p_k^* is the dimensionless pressure, $\mathbf{1}$ is the unit tensor, $\mathbf{T}_\mathbf{k}^{\mathbf{E}*} = 2\eta_k^*\mathbf{D}_k^*$ is the viscous part of the stress tensor, and $\mathbf{D}_k$ is the symmetric part of the velocity gradient. Since phase 1 obeys a Papanastasiou's equation and phase 2 is Newtonian, Eq. 2 takes the form

$$-\nabla^* p_1^* + \frac{1}{N_\eta}\nabla^* \cdot \left\{1 - \tau_0' + \frac{\tau_0'}{\dot\gamma_1^*}\left[1 - \exp(-\alpha^*\dot\gamma_1^*)\right]\right\}\mathbf{D}_1^* = 0, \tag{3}$$

in the displacing fluid domain, and

$$-\nabla^* p_2^* + \nabla^* \cdot \mathbf{D}_2^* = 0, \tag{4}$$

in the displaced fluid domain. The quantity $\dot\gamma_1 \equiv \sqrt{(1/2)\mathrm{tr}\,(2\mathbf{D}_1)^2}$ is the intensity of the deformation rate tensor, and the dimensionless quantities labeled with a superscript $*$ are given by

$$\nabla^* \equiv H_0\nabla; \quad p_k^* \equiv \frac{p_k H_0}{\mu_2 U}; \quad \alpha^* = \frac{\alpha U}{H_0}; \quad \dot\gamma_1^* \equiv \frac{\dot\gamma_1 H_0}{U};$$
$$\mathbf{D}_k^* \equiv \frac{2H_0}{U}\mathbf{D}_k. \tag{5}$$

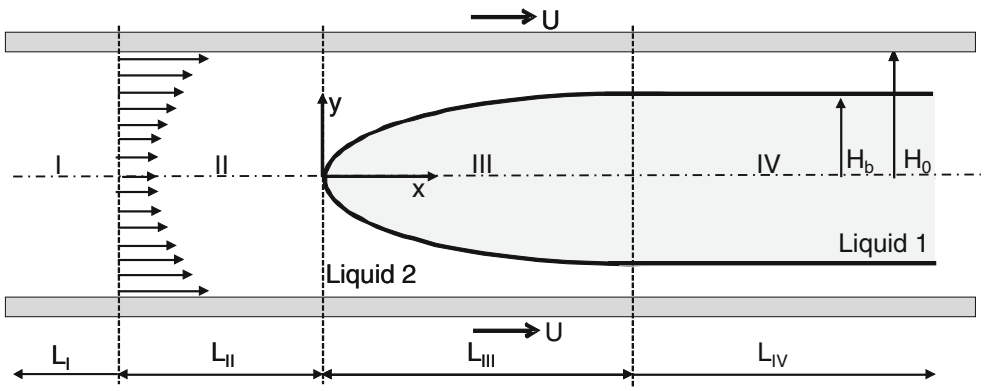

Fig. 2 Scheme of the problem

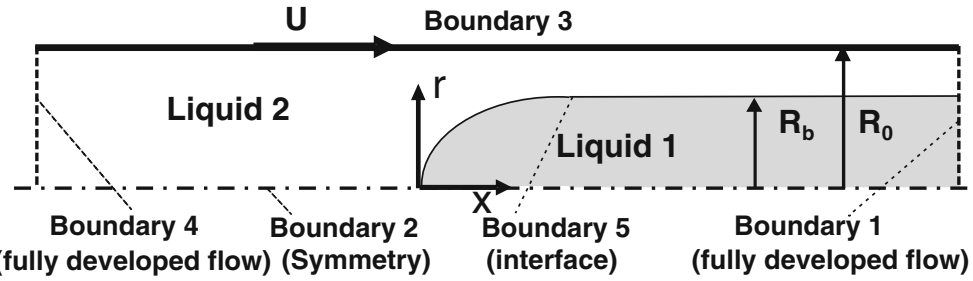

Fig. 3 Boundary conditions of the problem

In Eq. 3, we see the presence of the viscosity ratio, N_η, and the yield number, τ_0'. The characteristic viscosity of the displacing fluid was taken as the Bingham viscosity evaluated at the characteristic deformation rate U/H_0. Hence, N_η is given by

$$N_\eta = \frac{\mu_2}{\tau_0 \frac{H_0}{U} + \mu_p}, \tag{6}$$

and the yield number has the following expression:

$$\tau_0' = \frac{\tau_0}{\tau_0 + \mu_p \frac{U}{H_0}}. \tag{7}$$

When $\tau_0 = 0$, the Newtonian–Newtonian liquid displacement, presented by Freitas et al. (2011), is recovered. When $N_\eta \to \infty$, the gas liquid displacement is recovered.

Boundary conditions

We labeled the boundaries from 1 to 5 (see Fig. 3). Boundary 4, the flow is taken to be fully developed and the pressure is assumed to be uniform. Hence,

$$\mathbf{n} \cdot \nabla \mathbf{u}_2^* = 0, \qquad p_2^* = P_{in}^*, \tag{8}$$

where $\mathbf{n}$ is the unit vector normal to the boundary surface, and p_2^* is the constant dimensionless pressure field on phase 2 at the inlet. Downstream, far from the tip of the interface, boundary 1, the flow is also assumed to be fully developed with a uniform pressure imposed, which leads to

$$\mathbf{n} \cdot \nabla^* \mathbf{u}_k^* = 0, \qquad p_k^* = P_{\text{out}}^*. \tag{9}$$

Along the symmetry axis, boundary 2, both the shear stress and the velocity component v vanish. Hence,

$$\mathbf{n} \cdot [\mathbf{T}_k^* \cdot \mathbf{t}] = 0, \qquad \mathbf{n} \cdot \mathbf{u}_k^* = 0, \tag{10}$$

where $\mathbf{t}$ is a unit vector tangent to the boundary surface. No-slip and impermeability conditions are imposed along the tube wall, boundary 3. Therefore,

$$\mathbf{u}_2^* = \mathbf{e}_x, \tag{11}$$

where $\mathbf{e}_x$ is the unit vector in the x-direction. At the liquid–liquid interface, boundary 5, the traction balances the capillary pressure, and there is no mass flow across the interface. These conditions can be translated by

$$\mathbf{u}_1^* = \mathbf{u}_2^* = \left(\mathbf{u}_k^* \cdot \mathbf{t}\right) \mathbf{t}, \tag{12}$$

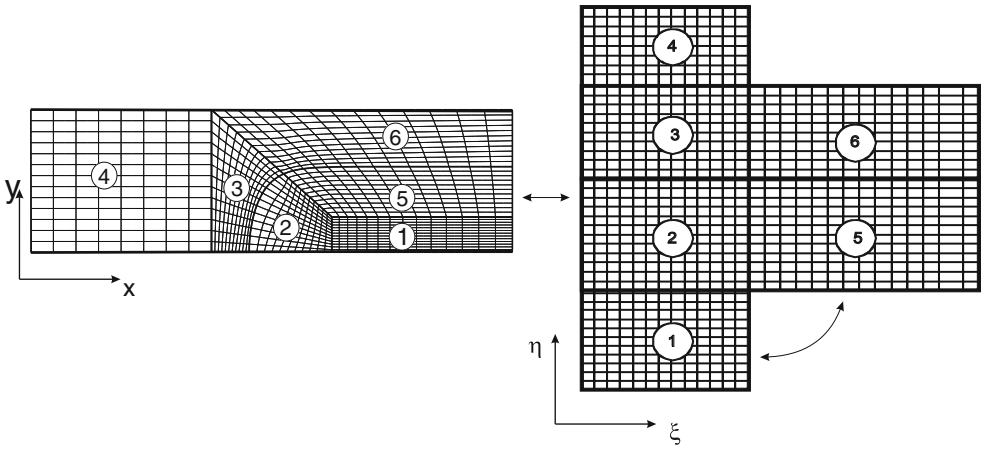

Fig. 4 Mapping between reference and physical domains

Fig. 5 Typical mesh

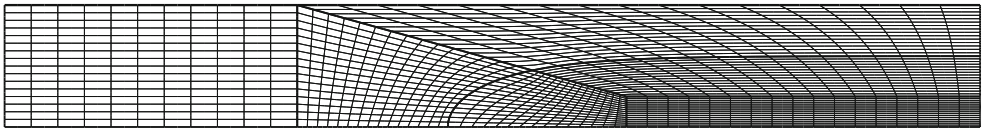

where **t** is the tangent vector, which states that there is no flux crossing the interface. Besides that, at this same boundary 5, the traction balances the capillary pressure,

$$\mathbf{n}(p_1^* - p_2^*) + \mathbf{n} \cdot \left\{ \mathbf{D_2^*} - \frac{1}{N_\eta} \left[1 - \tau_0' + \frac{\tau_0'}{\dot{\gamma}_1^*} \left[1 - \exp(-\alpha^* \dot{\gamma}_1^*) \right] \right] \mathbf{D_1^*} \right\} = \frac{1}{\mathrm{Ca}} \frac{1}{R_m^*} \mathbf{n}, \tag{13}$$

where p_1^* and p_2^* are the dimensionless pressures on phases 1 and 2, the capillary number Ca is given by

$$\mathrm{Ca} = \frac{\mu_2 U}{\sigma}, \tag{14}$$

where σ is the liquid–liquid interfacial tension. $R_m^* = R_m/H_0$ is the dimensionless radius of curvature. Equation 13 carries the dimensionless numbers that govern the problem, namely Ca, N_η, and the rheological parameter τ_0'.

When $\tau_0' = 0$, Eq. 13 assumes the form of the Newtonian–Newtonian liquid displacement, with $N_\eta = \mu_2/\mu_p$, and when $N_\eta \to \infty$, the gas–liquid displacement problem is recovered. In the limit Ca$\to \infty$, the stress is continuous through the interface and Eq. 13 shows the jump of the strain rate from one phase to the other.

Numerical implementation

The details concerning the elliptic grid generation, the solution of the equation system by Galerkin finite element method, including the basis functions used to represent position, velocity, and pressure are described in Soares and Thompson (2009) with some adaptation to cartesian coordinates. Since the domain of the problem is part of the solution, the problem is formulated in a reference domain and mapped onto the physical domain as shown in Fig. 4. For the solution of the nonlinear system of algebraic equations by Newton's method, a frontal solver was used. The initial guess to solve the Newtonian displacement of a viscoplastic material was the Newtonian–Newtonian displacement with the same viscosity ratio. Figure 5 shows a typical mesh used in our simulations.

Results and discussion

The main results of the present work were obtained using $\alpha^* = 1{,}000$, as recommended in the literature (e.g. Zou et al. 2008). We have also conducted a study of the sensitiveness of a sample of these results for other values of the dimensionless regularization parameter, which are shown in the last subsection, after the main results are presented. We have chosen viscosity ratios $N_\eta = 4$ and $N_\eta = 8$ in order to compare with the Newtonian results obtained by Freitas et al. (2011) and to avoid the limiting viscosity ratio which could lead to instabilities in the sense discussed by Lac and Sherwood (2009) and Soares and Thompson (2009).

In order to maintain the main aspects of the topology of the mesh keeping the tip of the interface at the same position for different cases, the difference $P_{\mathrm{in}}^* - P_{\mathrm{out}}^*$ had to be controlled and changed. Below we show two tables discriminating typical values for this difference (Table 1).

Displacement efficiency

The residual mass fraction, $m = 1 - \frac{H_b}{H_0}$, as a function of the capillary number, is shown in Figs. 6 and 7 for viscosity ratios $N_\eta = 4$ and $N_\eta = 8$, respectively. The different curves are related to different levels of yield number, from the Newtonian fluid ($\tau_0' = 0$) to

Table 1 Values of the difference $P_{\mathrm{in}}^* - P_{\mathrm{out}}^*$ for different capillary and yield numbers displayed for two values of viscosity ratio, $N_\eta = 8$ and $N_\eta = 4$

	$N_\eta = 8$			$N_\eta = 4$		
	$\tau_0' = 0.2$	$\tau_0' = 0.4$	$\tau_0' = 0.8$	$\tau_0' = 0.2$	$\tau_0' = 0.4$	$\tau_0' = 0.8$
Ca = 10	11.60	11.20	10.64	13.80	13.36	12.28
Ca = 1	13.40	13.20	11.92	14.48	14.32	13.80
Ca = 0.1	26.80	26.00	25.60	28.40	27.80	27.32

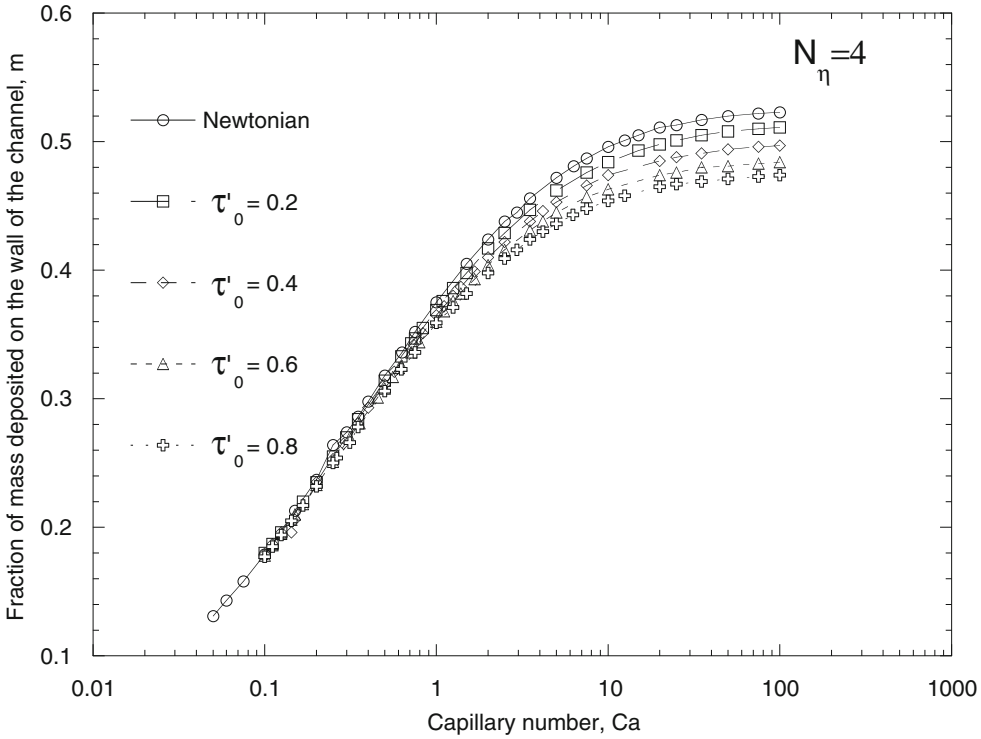

Fig. 6 Fraction of mass attached to the wall as a function of the capillary number for different values of yield number and a fixed viscosity ratio, $N_\eta = 4$

a Papanastasiou's material with $\tau_0' = 0.8$ (where $0 \leq \tau_0' < 1$). For small values of capillary number, Ca < 1, the variation of the yield number has no significant effect on the fraction of mass attached to the wall. The same happens when we compare the two figures, i.e., the viscosity ratio does not affect m for low values of the Ca. This results reinforces previous ones as those presented by Soares and Thompson (2009), Thompson and Soares (2010), and Freitas et al. (2011), where the rheological parameters have a weak influence when

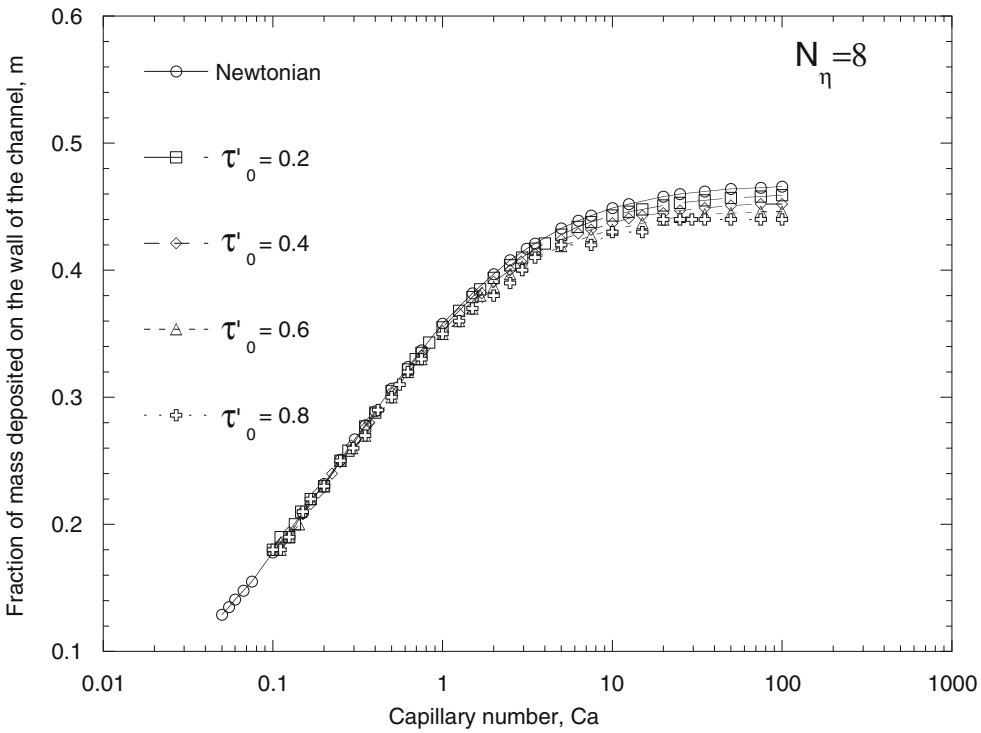

Fig. 7 Fraction of mass attached to the wall as a function of the capillary number for different values of yield number and a fixed viscosity ratio, $N_\eta = 8$

the interfacial tension becomes significant (when the capillary number is small). Figures 6 and 7 also show that as the yield number increases, the residual fraction of mass decreases. As shown in some previous works, e.g., Sousa et al. (2007) and Thompson et al. (2010), there is a strong qualitative similarity between the effects caused by an increase in the yield number and a decrease in the power-law index in pseudoplastic fluids. This same qualitative tendency can be verified if we compare the results presented in Figs. 6 and 7 to the ones presented by Thompson and Soares (2010) for power-law fluids displacing Newtonian ones (although in that case it was investigated in the context of the capillary tube problem). As reported by that study, for viscosity-thinning fluids, when the power-law index is decreased, the fraction of mass attached to the wall also decreases.

The influence of viscosity ratio was already explored by Freitas et al. (2011). When the viscosity ratio is increased, the residual mass fraction decreases. The new aspect shown in Figs. 6 and 7 is the fact that high values of viscosity ratio inhibits the influence of the yield number. The main qualitative effects, on the residual mass fraction, obtained from changing yield number or viscosity ratio can be explained by the dimensionless form of the force balance at the interface, Eq. 13. The deformation rate jump at the interface in region IV (see Fig. 2) is given by

$$\mathbf{n}\cdot\mathbf{D}_2^*(H_b)\cdot\mathbf{t} = \frac{1}{N_\eta}\left\{1-\tau_0'+\frac{\tau_0'}{\dot{\gamma}_1^*(H_b)}\left[1-\exp[-\alpha^*\dot{\gamma}_1^*(H_b)]\right]\right\}\mathbf{n}\cdot\mathbf{D}_1^*(H_b)\cdot\mathbf{t}, \quad (15)$$

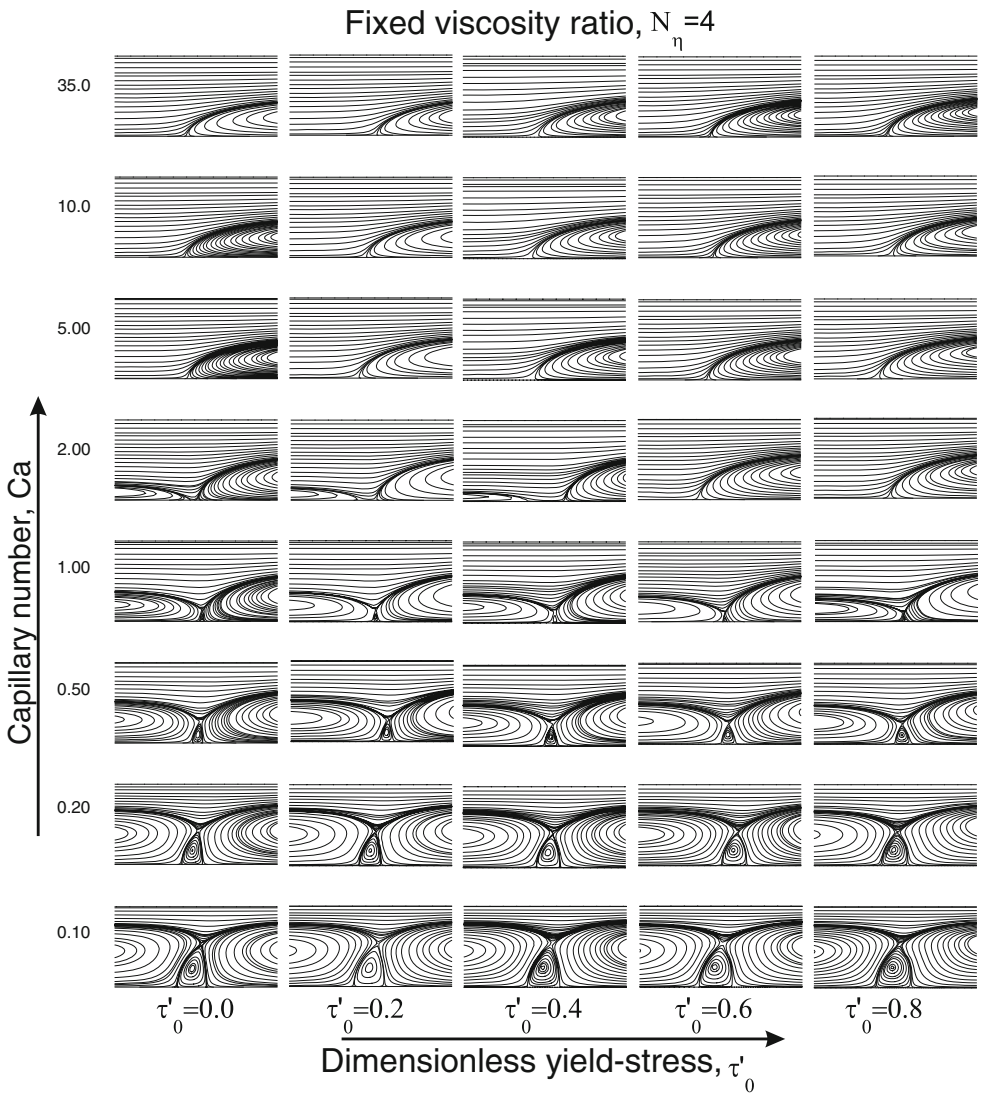

Fig. 8 Flow patterns disposed in the space (τ_0', Ca) for a viscosity ratio, $N_\eta = 4$

and can be approximated, for a high value of the dimensionless regularization parameter α^*, by

$$\mathbf{n}\cdot\mathbf{D}_2^*(H_b)\cdot\mathbf{t}=\frac{1}{N_\eta}\left[1-\tau_0'+\frac{\tau_0'}{\dot{\gamma}_1^*(H_b)}\right]\mathbf{n}\cdot\mathbf{D}_1^*(H_b)\cdot\mathbf{t}. \tag{16}$$

Since near the interface the deformation rate is significant, $\tau_0' < \tau_0'\dot{\gamma}_1^*(H_b)$. Hence, Eq. 16 shows that yield number and viscosity ratio have similar qualitative influences on the position of the interface, in the sense that they affect the deformation rate jump at the interface in the same direction, i.e., increasing N_η or τ_0' causes the deformation rate jump to decrease. Equations 15 or 16 also explains how a high value of viscosity ratio can lead to a negligible influence of the tangential forces at phase 1 side. When the viscosity ratio is very large, this problem tends to mimic the problem of a gas (in fact a inviscid fluid) displacing a Newtonian fluid no matter how complex is the rheology of displacing fluid if it is a GNF. Hence, these equations lead to a vanishing shear rate at the interface at region IV (where the flow is fully developed). Equation 16 has a strong similarity with the equivalent one presented by Thompson and Soares (2010) for the problem of a power-law fluid displacing a Newtonian one.

Maps of flow regimes

Figures 8 and 9 show some flow patterns disposed in a cartesian manner in the space (τ_0', Ca) for the values of viscosity ratios $N_\eta = 4$ and $N_\eta = 8$, respectively. We can observe that higher values of yield number induce

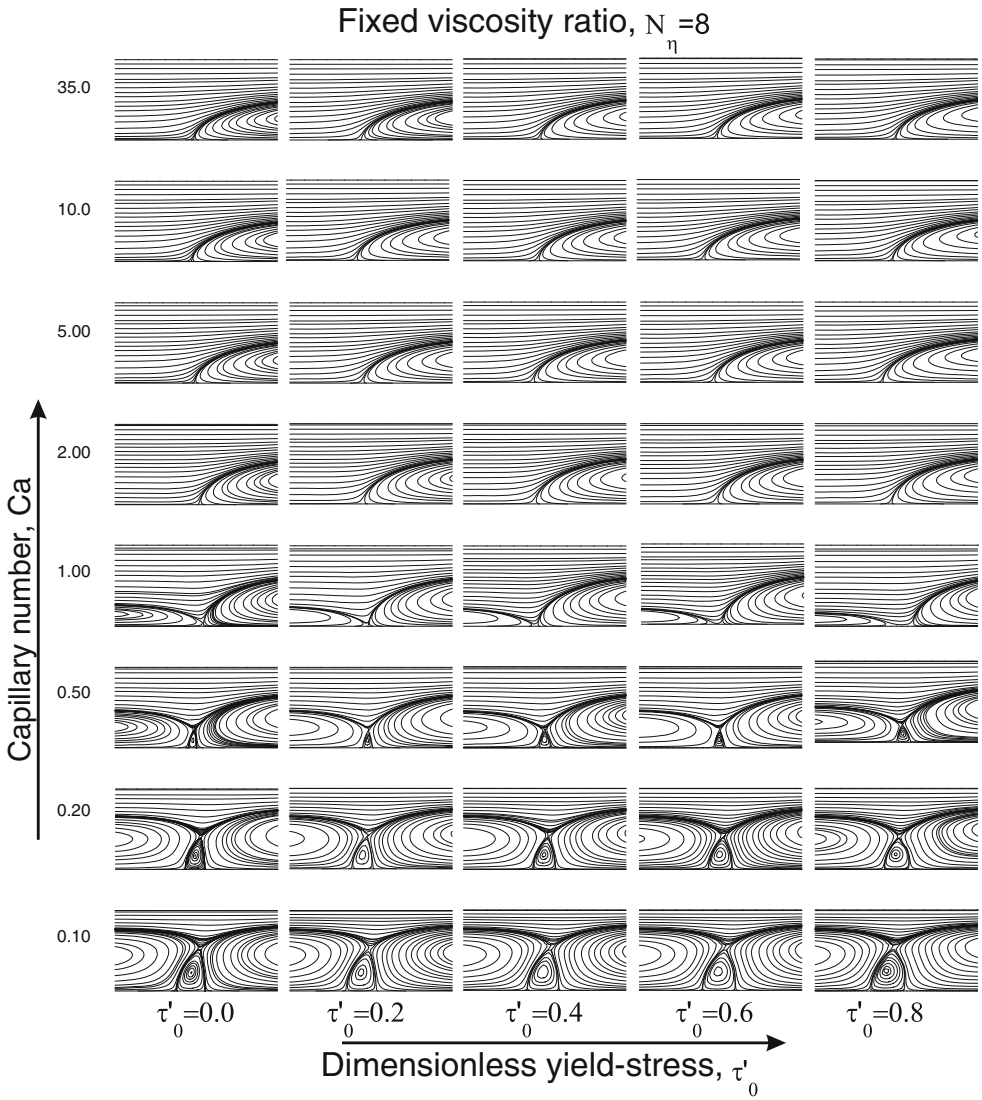

Fig. 9 Flow patterns disposed in the space (τ_0', Ca) for a viscosity ratio, $N_\eta = 8$

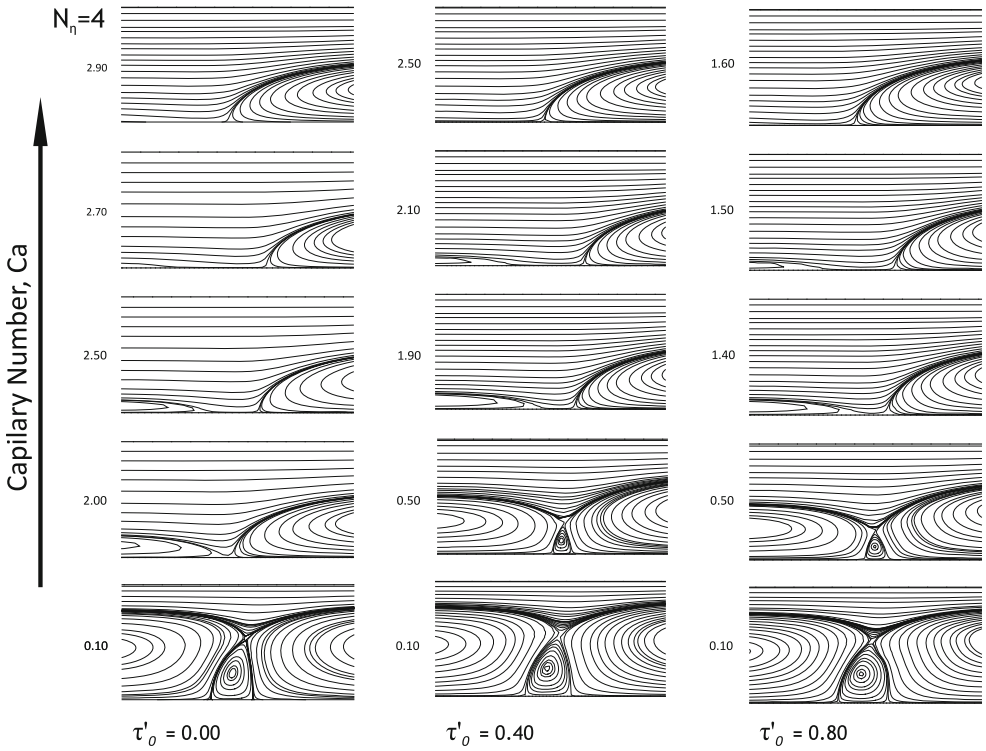

Fig. 10 Capillary number in the vicinity of the transition pattern for different levels of yield number with viscosity ratio, $N_\eta = 4$

bypass flow regimes, i.e., when there is no recirculation on the displaced fluid domain. Similarly to the results presented by Freitas et al. (2011), the viscosity ratio influences the flow regimes of the problem in the following way: higher values of N_η also induces bypass flow regimes.

The critical condition that marks the boundary between the bypass regime and the transition regime is

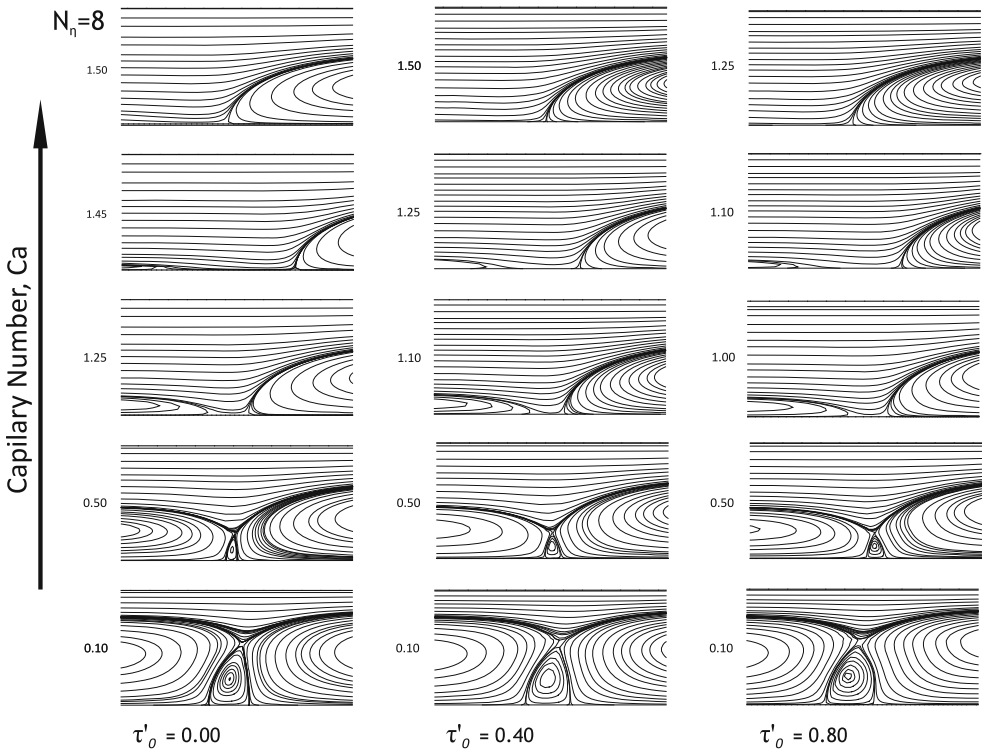

Fig. 11 Capillary number in the vicinity of the transition pattern for different levels of yield number with viscosity ratio, $N_\eta = 8$

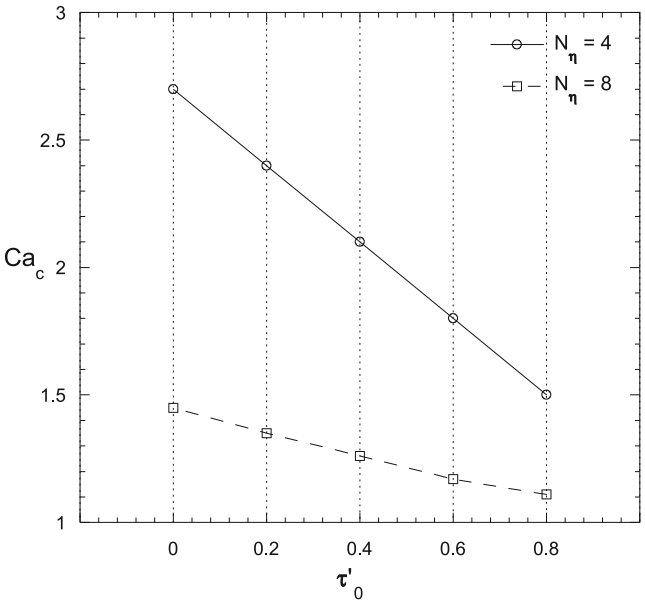

Fig. 12 Critical capillary number as a function of the yield number for viscosity ratios, $N_\eta = 4$ and $N_\eta = 8$

ruled by a competition between the moving wall and the pressure gradient influences. While the first tends to arrest phase 2 to the right, the second pushes the same fluid to the left. Therefore, in a bypass flow regime, the moving wall effect overcomes the pressure gradient one. When the pressure gradient is increased, there is a point where both influences are equal at the centerline. This set of parameters leads to the limit between bypass and transition patterns. If we increase again the pressure gradient, recirculating flow patterns are formed in the displacing fluid domain.

The influences of viscosity ratio and yield number, from the perspective of the flow regimes of the problem, are in the same direction: decreasing one or the other (or both) increases the tendency of occurrence of a full-recirculating flow pattern. As discussed above, the reason for this same tendency is related to the influences of these rheological dimensionless parameters on the pressure gradient at region I. However, the pressure gradients at regions I and IV are related

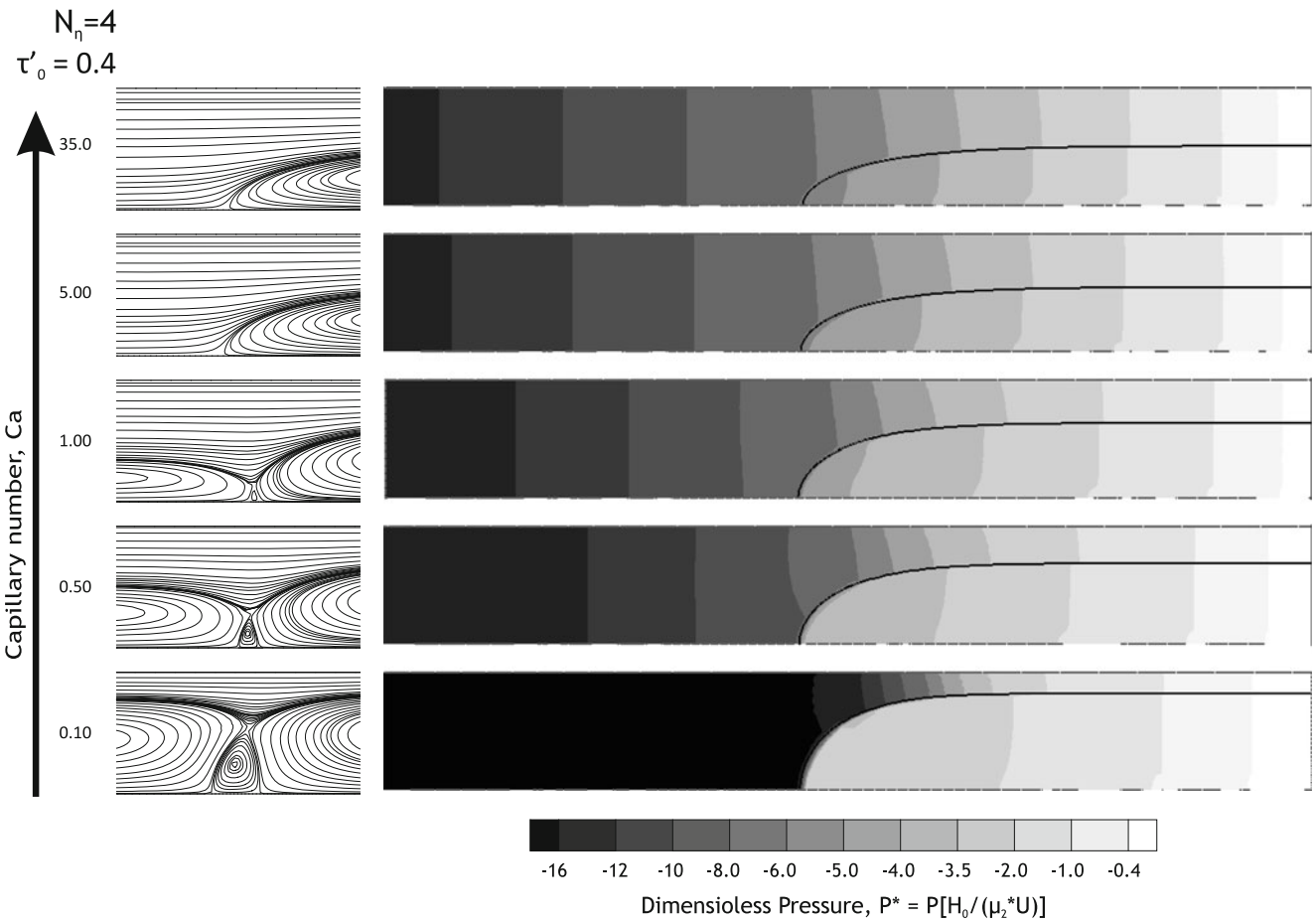

Fig. 13 Isoband pressure field for a viscosity ratio, $N_\eta = 4$, and a yield number, $\tau_0' = 0.4$, for different levels of capillary number covering the flow patterns the problem exhibit

by the continuity equation that leads to the following expression found by Freitas et al. (2011):

$$\left.\frac{\mathrm{d}p}{\mathrm{d}x}\right|_I^* = 1 - m + \left.\frac{\mathrm{d}p}{\mathrm{d}x}\right|_{IV}^* \left[\frac{1}{2}(1-m)^3 - \frac{3}{2}(1-m) + 1\right], \tag{17}$$

where $\left.\frac{\mathrm{d}p}{\mathrm{d}x}\right|_I^*$ and $\left.\frac{\mathrm{d}p}{\mathrm{d}x}\right|_{IV}^*$ are dimensionless pressure gradients at regions I and IV. The polynomial $\frac{1}{2}(1-m)^3 - \frac{3}{2}(1-m) + 1$ is positive for $0 < m < 1$ and, therefore,

$$\frac{\partial \left.\frac{\mathrm{d}p}{\mathrm{d}x}\right|_I^*}{\partial \left.\frac{\mathrm{d}p}{\mathrm{d}x}\right|_{IV}^*} > 0. \tag{18}$$

This result allows us to deviate the analysis to the pressure gradient at region IV. Since the curvature of the interface at this region vanishes, the pressure gradient at both fluids is the same. Analyzing from phase 1 perspective, Eq. 3, the dimensionless pressure gradient is given by

$$\nabla^* p_1^* = \frac{1-\tau_0'}{N_\eta}\nabla^* \cdot \mathbf{D}_1^* + \frac{\tau_0'}{N_\eta}\nabla^* \cdot \left[\frac{1-\exp(-\alpha^*\dot{\gamma}_1^*)}{\dot{\gamma}_1^*}\mathbf{D}_1^*\right]. \tag{19}$$

If α^* has a high value, as it should be to mimic a plastic behavior, the last divergent term can be approximated by

$$\frac{\tau_0'}{N_\eta}\nabla^* \cdot \left[\frac{1-\exp(-\alpha^*\dot{\gamma}_1^*)}{\dot{\gamma}_1^*}\mathbf{D}_1^*\right] \approx \frac{\tau_0'}{N_\eta}\nabla^* \cdot \left(\frac{\mathbf{D}_1^*}{\dot{\gamma}_1^*}\right) = \mathbf{0}, \tag{20}$$

where the last equality is due to the fact that the intensity and the dyadic direction of tensor $\frac{\mathbf{D}_1^*}{\dot{\gamma}_1^*}$ is constant at region IV. Equation 19 can be rewritten as the approximation:

$$\left[\nabla^* p_1^*\right]_{IV} \approx \frac{1-\tau_0'}{N_\eta}\left[\nabla^* \cdot \mathbf{D}_1^*\right]_{IV}, \tag{21}$$

and shows that increasing N_η or τ_0', $\nabla^* p_1^*$ decreases. That's why high values of viscosity ratio and yield number lead to bypass flow regimes. These kind of change inhibits the pressure gradient influence.

From Figs. 8 and 9, we can identify the rough location of critical capillary number, Ca_c, and of critical yield number, τ_{0c}', for viscosity ratios $N_\eta = 4$ and $N_\eta = 8$, respectively. When $N_\eta = 4$, $\tau_0' \leq 0.4 \Rightarrow 2.00 < \mathrm{Ca}_c <$

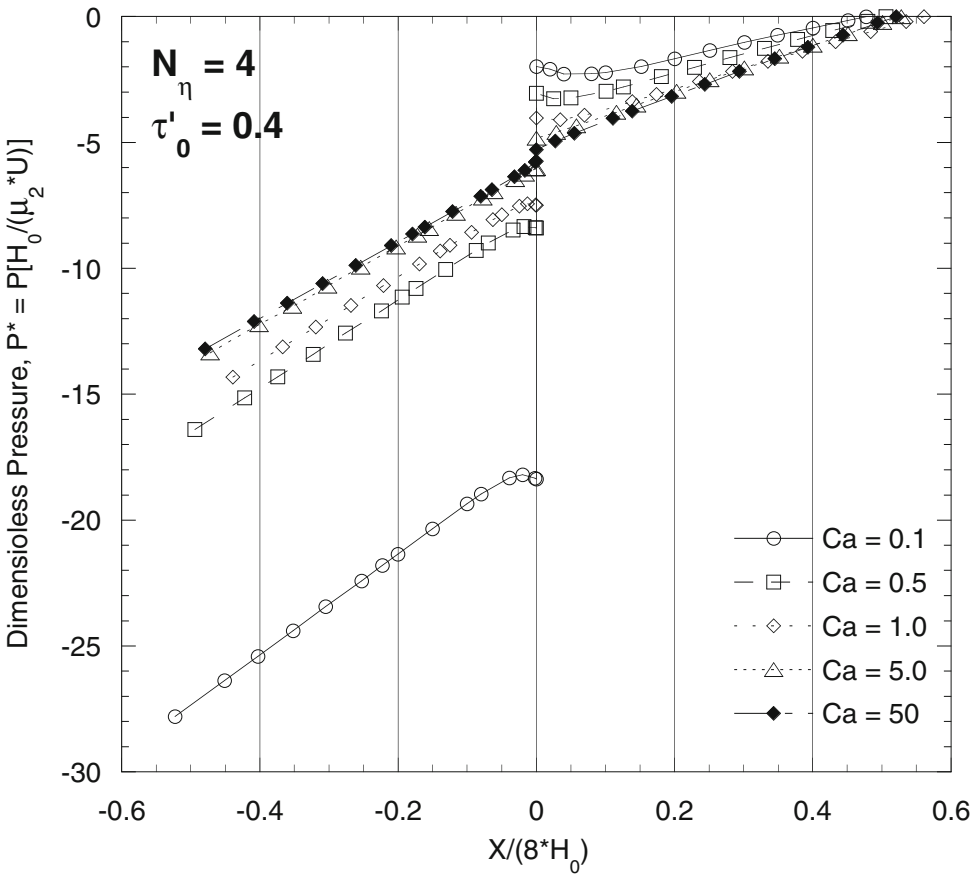

Fig. 14 Dimensionless pressure at the centerline for a viscosity ratio, $N_\eta = 4$, and a yield number, $\tau_0' = 0.4$

5.00 and $0.4 < \tau_0' \leq 0.8 \Rightarrow 1.00 < \mathrm{Ca}_c < 2.00$; while for $N_\eta = 8$, $1.00 < \mathrm{Ca}_c < 2.00$ for any $\tau_0' \leq 0.8$.

Refinement on transition flow patterns

For a more precise location of the transition regimes and a better understanding of its nature, we refine the value of capillary number for some fixed values of N_η and τ_0' as depicted in Figs. 10 and 11. Differently from the transition flow patterns presented in Sousa et al. (2007) and Thompson et al. (2010), we can observe that the kinds of transition regimes obtained are similar to the ones sketched by Taylor (1961), i.e. taking the bypass regime as reference, the recirculation emerges in the displaced fluid domain far from the interface. We can notice that as the yield number increases, the values of Ca_c decreases. We can also observe that there is a significant difference between the values of critical capillary number when we compare the two viscosity ratios analyzed, namely $N_\eta = 4$ and $N_\eta = 8$, for a fixed yield number. These results are summarized in Fig. 12.

Figures 13 and 14 show the pressure field for a viscosity ratio, $N_\eta = 4$, and a yield number, $\tau_0' = 0.4$. The different values of capillary number cover bypass, transition, and fully recirculating flow patterns. In Fig. 13, we can see that the pressure field has a significant change when a secondary recirculation is formed in the displacing fluid side. The pressure intensity at phase

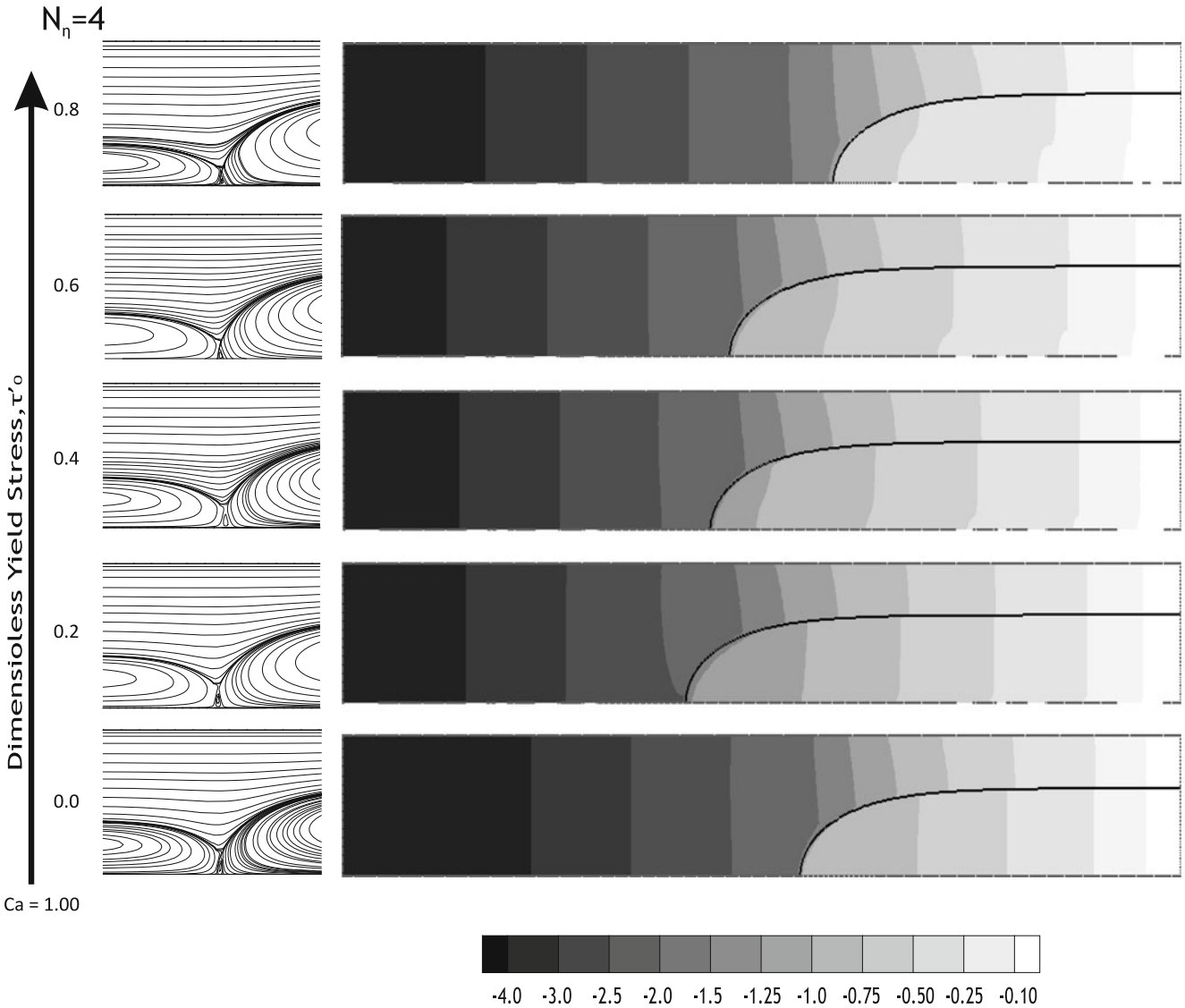

Fig. 15 Isoband pressure field for a viscosity ratio, $N_\eta = 4$, and a capillary number, $\mathrm{Ca} = 1$, for different levels of capillary number covering the flow patterns the problem exhibit

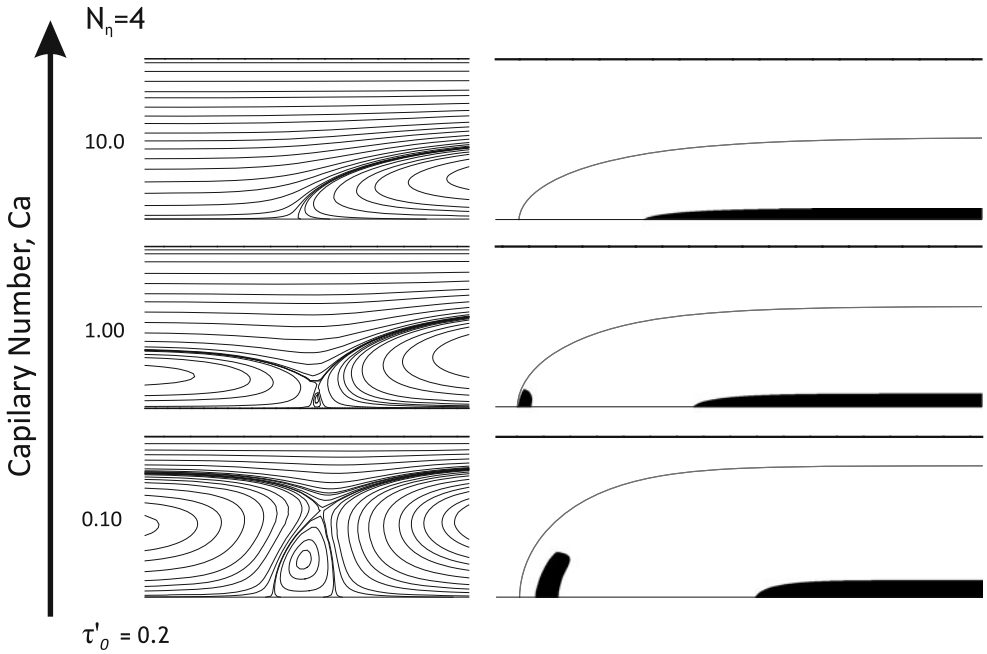

Fig. 16 Yielded and unyielded zones for a viscosity ratio, $N_\eta = 4$, and a yield number, $\tau_0' = 0.2$

2 side becomes higher and the isoband pressure fields near the tip become curved. Figure 14 shows the level of the pressure jump at the point of the tip of the interface. For a very high Ca, there is no significant change on the pressure gradient at the centerline. However, as the capillary number decreases, this difference becomes very important, i.e., the relative increase on the interface tension has a strong impact on the pressure jump. Figure 15 shows the pressure field for the same viscosity ratio, $N_\eta = 4$, and a capillary number, $\mathrm{Ca} = 1$, for different values of yield number. We can see that, as the yield number increases, the isoband pressure fields near the tip suffer a "diffraction" when passing from fluid to the other. The same effect is seen inside the displacing material domain. In this case, the origin of this phenomenon is the presence of an yield surface.

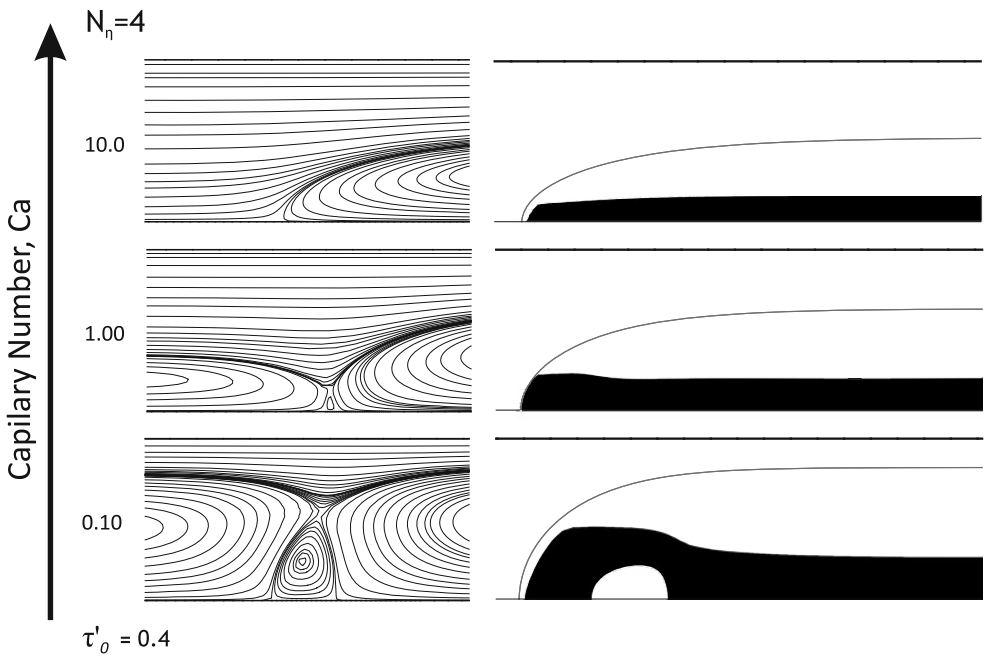

Fig. 17 Yielded and unyielded zones for a viscosity ratio, $N_\eta = 4$, and a yield number, $\tau_0' = 0.4$

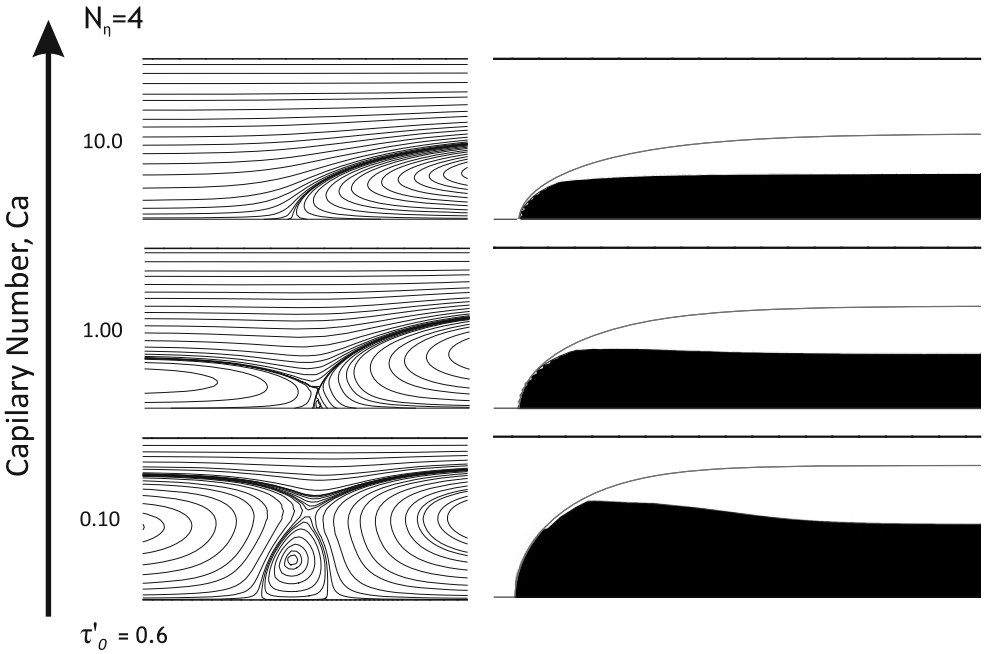

Fig. 18 Yielded and unyielded zones for a viscosity ratio, $N_\eta = 4$, and a yield number, $\tau_0' = 0.6$

Yielded and unyielded zones

In order to study the influence of capillary number and yield number on the location of the yield surface that limits yielded and unyielded zones of a viscoplastic material, we show, from Figs. 16, 17, 18, and 19, yielded, in white, and unyielded, in black, zones inside Phase 1 domain (phase 2 is Newtonian) for $N_\eta = 4$. We are showing these zones for 4 levels of yield number, correspondent to $\tau_0' = 0.2; 0.4; 0.6; 0.8$. The three cases, shown in each figure, correspond to the values of capillary number Ca = 0.1; 1; 10. These values were chosen so as the high capillary number value corresponds to a bypass regime, the low one corresponds to a full-recirculating regime, and the intermediate one corresponds to a regime near the transition. On the left of each figure, we can see the correspondent flow pattern near the tip of the drop.

As discussed in "Introduction," the Papanastasiou's equation does not give a yield surface in the traditional

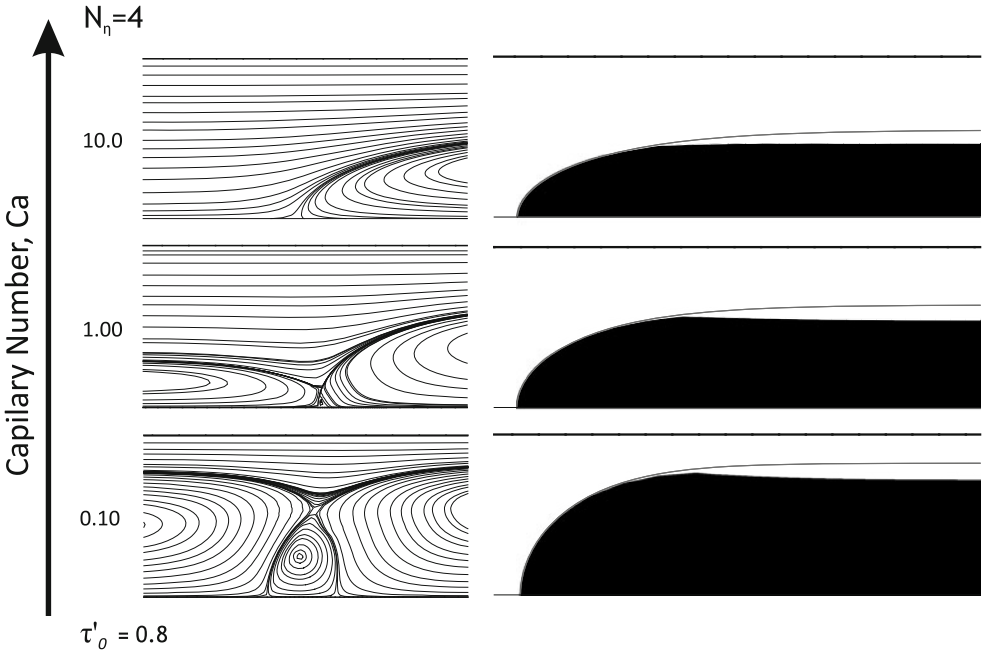

Fig. 19 Yielded and unyielded zones for a viscosity ratio, $N_\eta = 4$, and a yield number, $\tau_0' = 0.8$

sense, i.e., inside the unyielded zone, the deformation rate vanishes. In the present case, the yield surface, in this 2-D cartesian problem, is an isostress line determined by the level of intensity of the viscous stress tensor, $\mathbf{T}_E = \mathbf{T} + p\mathbf{1}$. It is the line where $\sqrt{0.5\mathrm{tr}\mathbf{T}_E^2} = \tau_0$.

Figure 16 shows yielded (in white) and unyielded (in black) zones for $N_\eta = 4$ and $\tau_0' = 0.2$. For the bypass regime correspondent to Ca = 10, there is only a thin unyielded zone near the centerline a bit far from the tip of the drop. For the case where Ca = 1, the recirculation at the displaced fluid reaches the interface, and a timid secondary recirculation is formed at the displacing fluid side. This timid recirculation is accompanied by a small unyielded zone. The unyielded zone near the centerline is farther from the tip. The smaller capillary number case, Ca = 0.1, also presents the same tendency. The full-recirculating pattern is accompanied by an increase on the unyielded zone near the tip, a change of position of the unyielded zone of the centerline to the opposite direction of the tip of the drop and an increase on the thickness of this layer.

When the yield number is $\tau_0' = 0.4$, with the same viscosity ratio, $N_\eta = 4$, as depicted in Fig. 17, an interesting phenomenon happens. While in the high and intermediate levels of capillary number, Ca = 10 and Ca = 1, the unyielded zones near the tip and at the centerline become a single simply connected one; for $Ca = 0.1$ there is an isle of yielded zone confined by an unyielded zone. Interestingly, it seems that the secondary recirculation that is formed in the displacing fluid increases the level of stress just after this recirculation. In other words, a change on the capillary number turns yielded zones to unyielded and vice versa. This fact shows that by decreasing the Ca, there are certain regions where the stress level decreases due to decrease of the stresses induced by viscous effects, but there are other regions where the stress level can increase due to an increase of the stresses induced by capillary effects.

When the yield number is increased to $\tau_0' = 0.6$, the three levels of capillary number present a simply connected unyielded zone from the tip of the interface to the region near the centerline. For Ca = 0.1, the unyielded zone near the tip is clearly influenced by the size of the secondary recirculation.

Yielded and unyielded zones with viscosity ratio, $N_\eta = 4$, for the highest level of yield number investi-

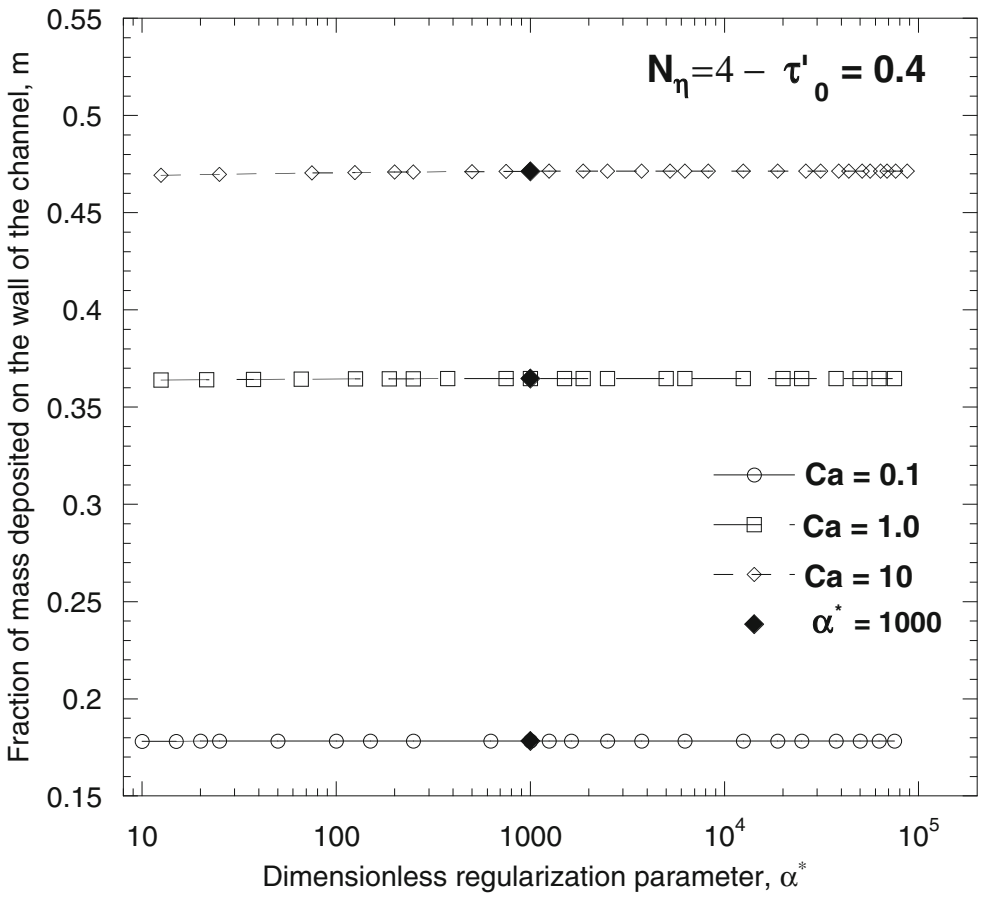

Fig. 20 Fraction of mass deposited on the wall for a viscosity ratio, $N_\eta = 4$, and a yield number, $\tau_0' = 0.4$, as a function of the regularization parameter, α^*, for the levels of capillary number, Ca = 0.1; 1.0; 10

gated, $\tau_0' = 0.8$, are shown in Fig. 19. Here, we can see that the yielded zone is confined to the region that is very near the interface, at region IV. In this case, the flow regime and the position of the interface are more sensitive to a change on the capillary number.

The qualitative aspects of the determination of yielded and unyielded zones for the higher value of viscosity ratio, $N_\eta = 8$, are the same ones discussed for $N_\eta = 4$ and does not bring any new insight to the problem.

It should be mentioned that the obtained recirculations inside unyielded zones are only possible due to the Papanastasiou's modification of the Bingham material. In fact, we have a region of very small deformation rate that leads to a small level of stress, below τ_0. In this case, we can only interpret this result as physical if we consider a Papanastasiou model as a model on its own right (and not a model conceived to reproduce Bingham materials), i.e., if we consider that these results come from a Papanastasiou material. Another important point to address is that the unyielded zones formed near the centerline are far from the point where the velocity vanishes. A similar result was obtained by Mitsoulis and Zisis (2001) for the lid cavity: the unyielded zone is not centered in the eye of the recirculation.

Sensitiveness to the dimensionless regularization parameter

Figures 20 and 21 show the residual fraction of mass, m, as a function of the dimensionless regularization parameter, α^*, for a fixed viscosity ratio, $N_\eta = 4$. While in Fig. 20, the yield number is fixed in $\tau_0' = 0.4$ and there are three different values of capillary number, $\mathrm{Ca} = 0.1$, $\mathrm{Ca} = 1.0$, and $\mathrm{Ca} = 10$, in Fig. 21, the capillary number is fixed in $\mathrm{Ca} = 1$ and there are three different values of yield number, $\tau_0' = 0.2$, $\tau_0' = 0.4$, and $\tau_0' = 0.8$. There is no apparent difference between the cases analyzed. Even for the lowest value of α^*, the fraction of mass that remains attached to the wall is

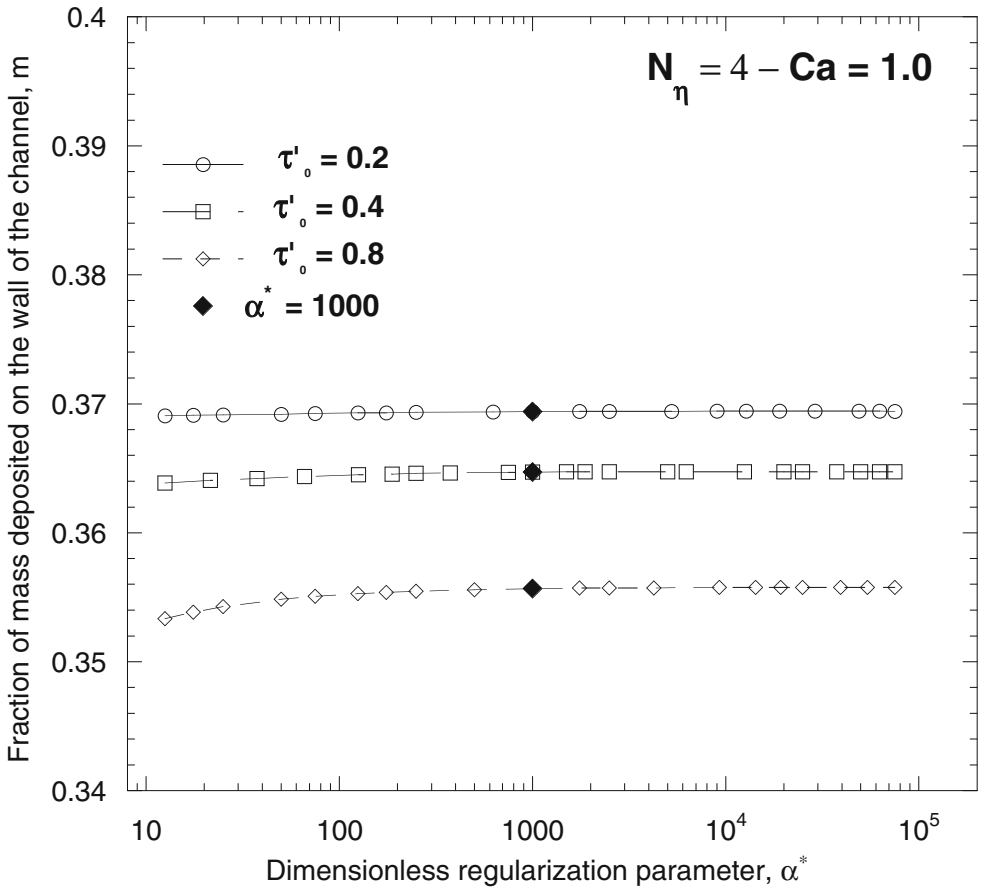

Fig. 21 Fraction of mass deposited on the wall for a viscosity ratio, $N_\eta = 4$, and capillary number, $\mathrm{Ca} = 1.0$, as a function of the regularization parameter, α^*, for the levels of yield number, $\tau_0' = 0.2; 0.4; 0.8$

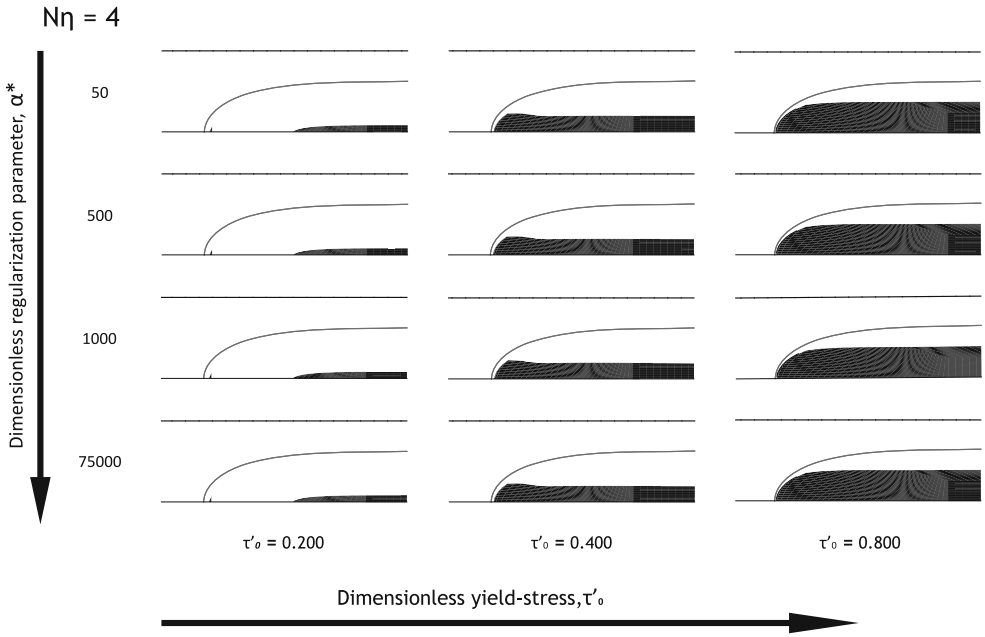

Fig. 22 Influence of the regularization parameter, α^* on the position of yield surfaces for a viscosity ratio, $N_\eta = 4$, and capillary number, Ca = 1.0 for the levels of yield number, $\tau_0' = 0.2; 0.4; 0.8$

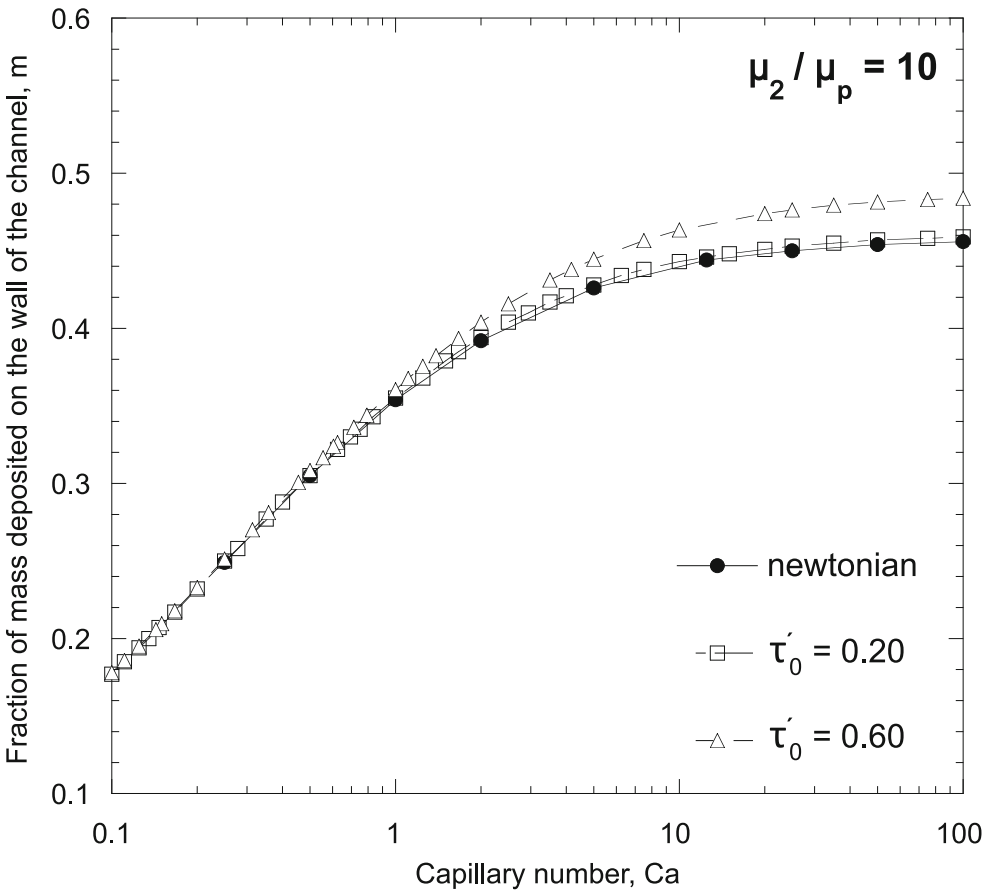

Fig. 23 Fraction of mass deposited on the plane channel walls for a fixed value of $N_{\mu p} = 10$

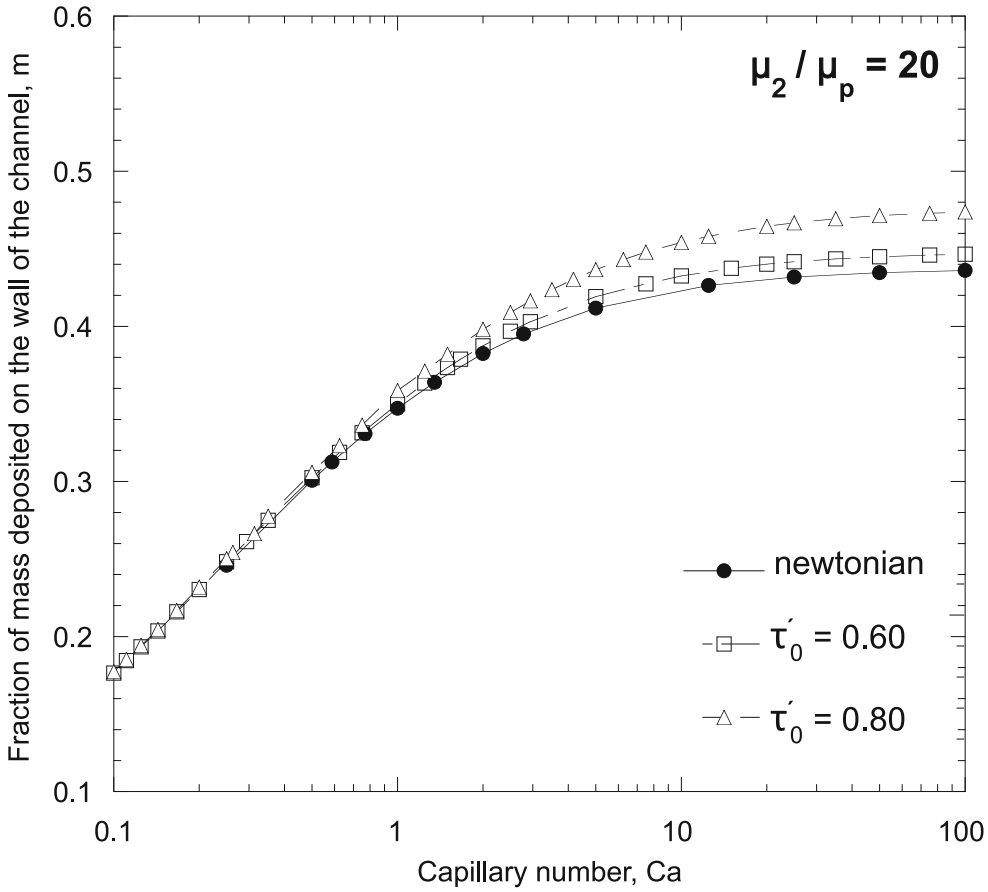

Fig. 24 Fraction of mass deposited on the plane channel walls for a fixed value of $N_{\mu p} = 20$

the same for a precision of 0.01. The only case that the difference can be detected as a visual curvature when α^* is changed is the case correspondent to the highest value of yield number, $\tau_0' = 0.8$. Even in this case, we can see that the value obtained with $\alpha^* = 1,000$ is not significantly altered for higher values of the dimensionless regularization parameter.

The same conclusion can be drawn for the fields of yielded and unyielded zones depicted in Fig. 22. As we can see, there is no significant change for the range of α^* investigated, namely from $\alpha^* = 50$ to $\alpha^* = 75,000$. It is difficult to distinguish one figure from the other.

Hence, we can conclude that, for the cases investigated, when $\alpha^* \geq 1,000$, the problem is virtually independent of this parameter.

Fraction of mass attached to wall when $\frac{\mu_2}{\mu_p}$ is maintained fixed—discussion

There are some investigations in the literature (e.g. Frigaard et al. 2007; Wielage-Burchard and Frigaard 2011), where a different choice of dimensionless numbers is employed, what can lead to apparent opposite conclusions. In the present work, the viscosity ratio is defined by Eq. 6, repeated here for convenience,

$$N_\eta = \frac{\mu_2}{\tau_0 \frac{H_0}{U} + \mu_p},$$

while Wielage-Burchard and Frigaard (2011), for example, define the viscosity ratio[1] as

$$N_{\mu p} = \frac{\mu_2}{\mu_p}. \tag{22}$$

The main motivation to adopt Eq. 22 is that the yield stress is only present on one single dimensionless number, namely Bingham (or yield) number. Therefore, this set of dimensionless numbers, $(N_{\mu p}, Bn)$ gives the possibility of seeing the effect of a change on the yield stress on the problem, by fixing $N_{\mu p}$. Figures 23 and 24 show such effect on the residual mass attached to the wall for different values of τ_0'. Comparing Figs. 23 and 24 with Figs. 6 and 7, one would find that from the pair

[1] In fact, in that case, there is a Newtonian displacement of a viscoplastic material, and so they define the viscosity ratio as $N_{\mu p} = \frac{\mu_p}{\mu_1}$. Equation 22 is the way the viscosity ratio would have been defined if we had followed the same philosophy.

$(N_{\mu p}, \tau_0')$ we conclude that the *effect of viscoplasticity* is to increase m, while from the pair (N_η, τ_0'), the *effect of plasticity* is to decrease m. *Since a change on the yield stress changes the level of viscosity*, when adopting the pair (N_η, τ_0'), we isolate the part of the observed change that is related to a simple change on the level of viscosity.

The physical mechanism through which the residual fraction of mass decreases when the viscosity ratio increases is described by Soares and Thompson (2009). In essence, when the viscosity of the inner fluid is increased, there is a decrease on the velocity near the core. Since the velocity at the external wall is fixed and the outer fluid has a comparatively lower viscosity, it needs a higher layer in order to achieve the low velocity levels near the interface. When we maintain $N_{\mu p}$ fixed an increase on the yield stress also increases the viscosity of the displacing fluid and therefore, decreases N_η and produces the results depicted on Figs. 23 and 24.

Final remarks

The immiscible displacement in a capillary plane channel of a Newtonian liquid by a viscoplastic one that obeys a Papanastasiou's constitutive equation was numerically analyzed. We investigated the displacement efficiency, measured by the residual fraction of mass of the displaced fluid attached to wall, and the flow patterns of the problem as functions of the dimensionless parameters that govern the problem: the capillary number (Ca), the viscosity ratio of the two fluids (N_η), and the yield number (τ_0'). The numerical results showed that for a fixed viscosity ratio, the residual fraction of mass is a decreasing function of τ_0'. The force balance at the interface of region IV on its dimensionless simplified form, leads to the following result

$$\mathbf{n}\cdot\mathbf{D}_2^*(H_b)\cdot\mathbf{t} = \frac{1}{N_\eta}\left[1-\tau_0'+\frac{\tau_0'}{\dot{\gamma}_1^*(H_b)}\right]\mathbf{n}\cdot\mathbf{D}_1^*(H_b)\cdot\mathbf{t}, \tag{23}$$

and was used to explain such behavior. This equation also explains the reason why for high values of viscosity ratio, the effects of changing the yield number are less pronounced.

Stream function contours displayed in a Cartesian manner as functions of τ_0' and Ca for fixed viscosity ratio were shown in order to capture the rough conditions where the flow presents bypass, transition, and recirculating patterns. For displacing fluids with a higher yield number, there is a tendency to induce bypass flow regimes, especially for high Ca. The dimensionless simplified form of the momentum conservation equation, given by

$$\left[\nabla^* p_1^*\right]_{IV} \approx \frac{1-\tau_0'}{N_\eta}\left[\nabla^*\cdot\mathbf{D}_1^*\right]_{IV}, \tag{24}$$

shows how a change on viscosity ratio or yield number leads to the same qualitative result on the equation.

Some refinement on the specific critical capillary number value that marks the boundary between bypass and transition flow regimes were also presented. These results can be useful if one wants to reproduce transition flow patterns in an experimental investigation. Since the transition range is narrow, see Soares and Thompson (2009), a more precise location of its conditions can be a start for searching.

Yielded and unyielded zones were presented for different values of capillary number. Every time that the yield number was increased, the region of unyielded zone increased also. However, a change on a different parameter, such as Ca, could lead to turn certain regions from yielded to unyielded but turn other regions from unyielded to yielded. On one of these cases, a non-simply connected yielded zone appeared in the domain.

An analysis of the influence of the dimensionless regularization parameter α^* was conducted. The adopted value $\alpha^* = 1{,}000$ was satisfactory, i.e., there was no detectable difference in the results when this parameter was increased.

A discussion on the possible sets of dimensionless numbers was conducted in order to clarify why apparently opposite conclusions can be taken. In particular, a viscosity ratio can be chosen in two different ways: (a) the ratio of the viscosity of the Newtonian displaced fluid to the plastic viscosity of the viscoplastic material and (b) the ratio of the viscosity of the Newtonian displaced fluid to the characteristic viscosity of the viscoplastic material. We believe the second choice is more appropriate as discussed by Denn and Bonn (2011).

Acknowledgments We would like to thank the reviewers for their valuable suggestions that helped to increase the quality of the manuscript. This research was partially funded by grants from PETROBRAS S.A., ANP (Brazilian Petroleum Agency), CAPES (Brazilian Graduate Education Foundation), CNPq (Brazilian Research Foundation), and FAPERJ (Research Foundation of the state of Rio de Janeiro).

References

Alexandrou AN, Entov V (1997) On the steady-state advancement of fingers and bubbles in a Hele-Shaw cell filled by a non-Newtonian fluid. Eur J Appl Math 8:73–87

Allouche M, Frigaard IA, Sona G (2000) Static wall layers in the displacement in two visco-plastic fluids in a plane channel. J Fluid Mech 424:243–277

Barnes HA (1999) The yield-stress—a review of $\rho\alpha\nu\tau\alpha\ \rho\epsilon\iota$—everything flows? J Non-Newton Fluid Mech 81:133–178

Bingham EC (1916) An investigation of the laws of plastic flow. U.S. Bureau of Standards Bulletin 13:309–353

Bretherton FP (1961) The montion of long bubble in tubes. J Fluid Mech 10:166–188

Chen JD (1986) Measuring the film thickness surrounding a bubble inside a capillary. J Colloid Interface Sci 109:341–349

Cox BG (1962) On driving a viscous fluid out of a tube. J Fluid Mech 20:81–96

de Souza Mendes PR, Dutra ESS, Siffert JRR, Naccache MF (2007) Gas displacement of viscoplastic liquids in capillary tubes. J Non-Newton Fluid Mech 145:30–40

de Souza Mendes PR, Dutra ESS (2004) Viscosity function for yield-stress liquids. Appl Rheol 6:296–302

Denn MM, Bonn D (2011) Issues in the flow of yield-stress liquids. Rheol Acta. doi:10.1007/s00397-010-0504-3

Dimakopoulos Y, Tsamopoulos J (2003) Transient displacement of a viscoplastic material by air in straight and constricted tubes. J Non-Newt Fluid Mech 112:43–75

Dimakopoulos Y, Tsamopoulos J (2004) On the gas-penetration in straight tubes completely filled with a viscoelastic fluid. J Non-Newt Fluid Mech 117:117–139

Fairbrother F, Stubbs AE (1935) Studies in electro-endosmosis. Part VI: The "bubble-tube" method of measurement. J Chem Soc 1:527–539

Freitas JF, Soares EJ, Thompson RL (2011) Residual mass and flow regimes for the immiscible liquid–liquid displacement in a plane channel. Int J Multiphase Flow. doi:10.1016/j.ijmultiphaseflow.2011.03.003

Frigaard IA, Nouar C (2005) On the usage of viscosity regularisation methods for visco-plastic fluid flow computation. J Non-Newton Fluid Mech 127:1–26

Frigaard IA, Vinay G, Wachs A (2007) Compressible displacement of waxy crude oils in long pipeline startup flows. J Non-Newton Fluid Mech 147:45–64

Giavedoni MD, Saita FA (1997) The axisymmetric and plane cases of a gas phase steadily displacing a Newtonian liquid simultaneous solution of the governing equations. Phys Fluids 9:2420–2428

Goldsmith HL, Mason SG (1963) The flow of suspensions through tubes. J Colloid Sci 18:237–261

Hassager O, Lauridsen TL (1998) Singular behavior of power-law fluids in hele shaw flow. J Non-Newton Fluid Mech 29:337–346

Hodges SR, Jenseng OE, Rallison JM (2004) The motion of a viscous drop through a cylindrical tube. J Fluid Mech 501:279–301

Huzyak M, Koelling IA (1997) The penetration of a long bubble through a viscoelastic fluid in a tube. J Non-Newton Fluid Mech 71:73–88

Lac E, Sherwood JD (2009) Motion of a drop along the centerline of a capillary in a pressure-driven flow. J Fluid Mech 640:27–54

Lee G, Shaqfeh ESG, Khomami B (2002) A study of viscoelastic free surface by finite element method Hele-Shaw and slot coating flows. J Non-Newton Fluid Mech 117:117–139

Malekmohammadi S, Naccache MF, Frigaard IA, Martinez DM (2010) Buoyance driven slump flows of non-Newtonian fluids in pipes. J Pet Sci Eng 72:236–243

Martinez MJ, Udell KS (1989) Boundary integral analysis of the creeping flow of long bubbles in capillaries. J Appl Mech 56:211–218

Martinez MJ, Udell KS (1990) Axisymmetric creeping motion of drops through circular tubes. J Fluid Mech 210:565–591

Mitsoulis E, Zisis Th (2001) Flow of a Bingham plastics in a lid-driven square cavity. J Non-Newton Fluid Mech 101:173–180

Papaioannou J, Karapetsas G, Dimakopoulos Y, Tsamopoulos J (2009) Injection of a viscoplastic material inside a tube or between two parallel disks: conditions for wall detachment of the advancing front. J Rheol 53:1155–1191

Papanastasiou TC (1987) Flow of materials with yield-stress. J Rheol 31:385–404

Park CW, Homsky GM (1984) Two phase displacement in Hele-Shaw cells: theory. J Fluid Mech 139:291–308

Poslinski AJ, Oehler PO, Stokes VK (1995) Isothermal gas-assisted displacement of a viscoplastic liquid in tubes. Polym Eng Sci 35:877–892

Putz A, Frigaard IA, Martinez DM (2009) On the lubrication paradox and the use of regularization methods for lubrication flows. J Non-Newton Fluid Mech 163:62–77

Soares EJ, Carvalho MS, de Souza Mendes PR (2005) Immiscible liquid–liquid displacement in capillary tubes. J Fluids Eng 127:24–31

Soares EJ, Thompson RL (2009) Flow regimes for the immiscible liquid–liquid displacement in capillary tubes with complete wetting of the displaced liquid. J Fluid Mech 641:63–84

Sousa DA, Soares EJ, Queiroz RS, Thompson RL (2007) Numerical investigation on gas-displacement of a shear-thinning liquid and a visco-plastic material in capillary tubes. J Non-Newton Fluid Mech 144:149–159

Taghavi SM, Seon T, Martinez DM, Frigaard IA (2009) Buoyancy-dominated displacement flows in near-horizontal channels: the viscous limit. J Fluid Mech 639:1–35

Taylor GI (1961) Deposition of a viscous fluid on the wall of a tube. J Fluid Mech 10:161–165

Thompson RL, Soares EJ (2010) Fraction of mass attached to the wall in the liquid–liquid displacement in capillary tubes when the displacing liquid is a power-law non-Newtonian fluid. In: BCR-V, Brazilian conference on rheology, Rio de Janeiro, Brasil, 14–16 July

Thompson RL, Soares EJ, Bacchi RDA (2010) Further remarks on numerical investigation on gas-displacement of a shear-thinning liquid and a visco-plastic material in capillary tubes. J Non-Newton Fluid Mech 165:448–452

Westborg H, Hassager O (1989) Creeping motion of long bubbles and drops in capillary tubes. J Colloid Interface Sci 133:135–147

Wielage-Burchard K, Frigaard IA (2011) Static wall layers in plane channel displacement flows. J Non-Newton Fluid Mech 166(5–6):245–261

Zou Y, Huilgol RR, Mitsoulis E (2008) Application of the Lambert W function to steady shearing flows of the Papanastasiou model. Int J Eng Sci 46:799–808